Islamic University Journal of Applied Sciences (IUJAS)
jesc@iu.edu.sa
Volume VII, Issue I, 1 July 2025, Pages 27-43

Thermodynamic and Mechanistic Insights into Paracetamol Removal from Aqueous Solutions by Graphitic Carbon Nitride Nanosheets

Ayyob M. Bakry [1], Abdulmajeed M. Jabbari [2], Zeinhom H. Mohamed [1], Mohammed B. Hawsawi [3], Nasser Amri [1] and R E Azooz [1, *]

[1] Department of Physical Sciences, Chemistry Division, College of Science, Jazan University, P.O. Box. 114, Jazan 45142, Kingdom of Saudi Arabia.
[2] Department of Pharmaceutical Chemistry, College of Pharmacy, University of Hail, 81442, Hail, Saudi Arabia
[3] Department of Chemistry, Faculty of Science, Umm Al-Qura University, Makkah 21955, Saudi Arabia

*Corresponding author: (R E Azooz), *Email Address*: rramadan@jazanu.edu.sa

Abstract

This study explored the potential of raw graphitic carbon nitride (g-C_3N_4) as a low-cost adsorbent for removing paracetamol from water. The material's structure and properties were analyzed using various techniques, including X-ray diffraction (XRD), Fourier-transform infrared spectroscopy (FTIR), Ultraviolet visible (UV-Vis) spectroscopy, and Transmission electron microscopy (TEM). Factors affecting paracetamol adsorption, such as pH, contact time, adsorbent dosage, and initial paracetamol concentration, were investigated. The results showed that a maximum adsorption capacity of 1.1 mg/g was achieved at 25 ^oC within 60 minutes. Both Langmuir and pseudo-second-order models accurately described the adsorption behavior. Density functional theory (DFT) confirms the stability of the complex formed between Paracetamol and Graphitic carbon nitride (g-C_3N_4), and Molecular dynamics (MD) and FTIR confirm the stability of H-bond formation a high adsorption energy of – 38.640 x10^{-3} kcal/mol. These findings suggest that modified graphitic carbon nitride can be a promising, eco-friendly, and affordable adsorbent for removing pharmaceutical contaminants from water.

Keywords: Paracetamol, Adsorption, g-C_3N_4, Density functional theory, Molecular dynamics, Adsorption energy and Removal.

https://doi.org/10.63070/jesc.2025.002
Received 09 February 2025; Revised 25 April 2025; Accepted 08 May 2025.
Available online 16 May 2025.

Graphical Abstract

TOF

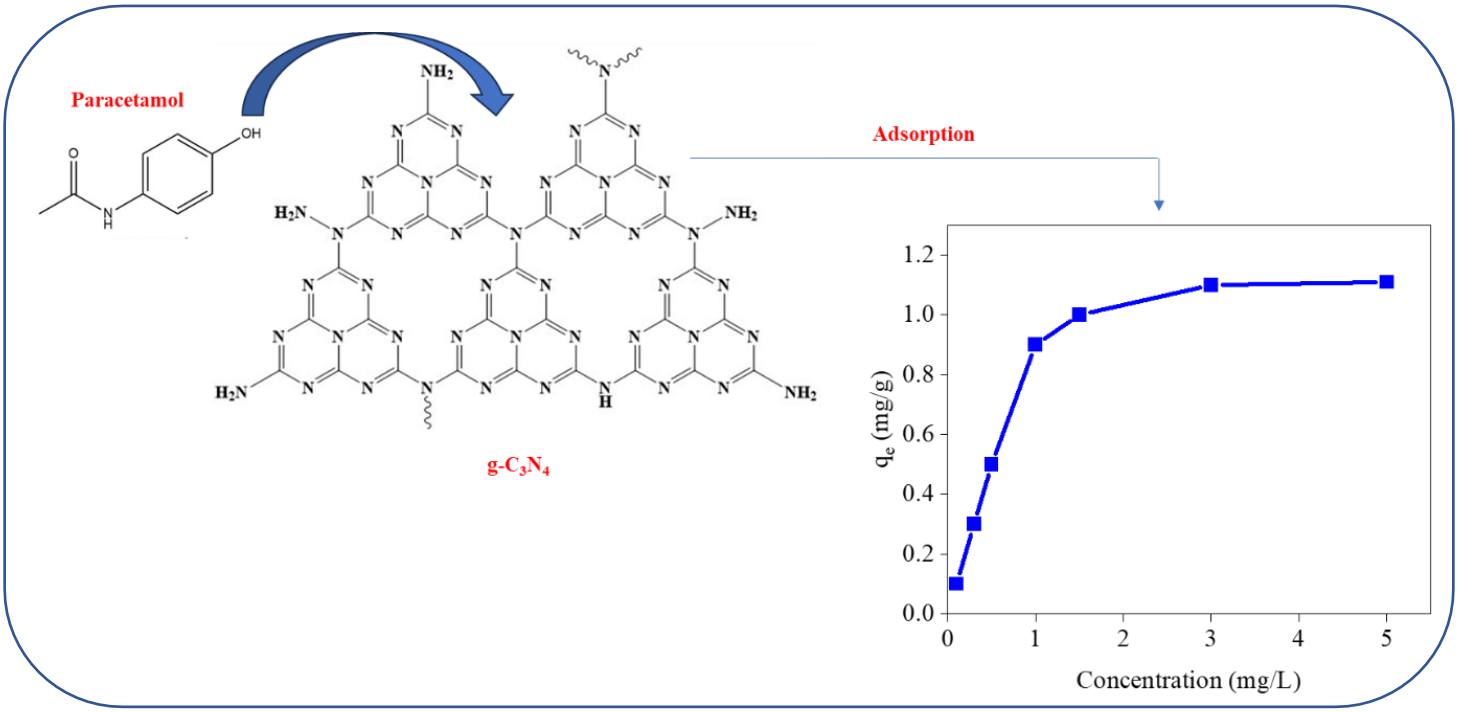

1. Introduction

Pharmaceutical water contamination is a global concern due to the widespread use of pharmaceuticals and their potential to pollute water sources. These contaminants can enter water bodies through various pathways, including wastewater discharges, improper disposal, and agricultural runoff. The presence of pharmaceuticals in water can have adverse effects on aquatic ecosystems, human health, and the environment.[1, 2] Pharmaceuticals can disrupt the hormonal balance of aquatic organisms, leading to reproductive issues and developmental abnormalities. In humans, exposure to contaminated water can have long-term health consequences, such as antibiotic resistance and endocrine disruption. Addressing pharmaceutical water contamination requires a multi-faceted approach, including improved wastewater treatment, proper medication disposal practices, and the development of sustainable pharmaceutical manufacturing processes.[2, 3] Among these contaminants, paracetamol is particularly concerning due to its frequent detection in water and wastewater. While concentrations may seem low, higher levels have been found in waste effluents, highlighting the need for effective removal methods to mitigate these environmental impacts.[4, 5]

Numerous techniques, such as photodegradation, membrane filtration, and ozonation, have been utilized for wastewater treatment.[5, 6] However, adsorption has emerged as a preferred method due to its simplicity, effectiveness, and environmental friendliness. This process involves the capture of pollutants onto the surface of an adsorbent material. One of the key advantages of adsorption is its versatility. Adsorbents can be modified to selectively target specific contaminants, like paracetamol, even in the presence of other molecules. This makes it particularly suitable for industrial wastewater treatment. Furthermore, adsorbed paracetamol can often be regenerated using appropriate eluents, allowing for the reuse of the adsorbent and reducing waste generation.[7, 8] A variety of materials have been explored for paracetamol adsorption, including activated carbon,[9] nitrogen-doped porous carbons,[10] and various frameworks.[11] The choice of adsorbent depends on factors like the specific properties of paracetamol and the desired water quality.

g-C_3N_4 is a promising alternative to activated carbon for adsorption applications. Unlike activated carbon, which is expensive and difficult to regenerate, g-C_3N_4 offers a more cost-effective and sustainable solution. This two-dimensional polymer boasts a honeycomb structure similar to graphene, composed of carbon and nitrogen atoms arranged in a triazine ring unit. This unique structure provides exceptional thermal and chemical stability, as well as a high surface area. The layered structure and abundant surface area of g-C_3N_4 create numerous binding sites for various molecules, making it an effective adsorbent. Moreover, the high nitrogen content of g-C_3N_4 enables strong interactions with pollutants, particularly those containing polar functional groups.[12-14] This combination of factors positions g-C_3N_4 as a promising adsorbent for a wide range of contaminants, including dyes, heavy metals, and organic pollutants from wastewater and air.

This study aimed to investigate the effectiveness of g-C_3N_4 as an adsorbent for removing paracetamol from aqueous solutions. Various experimental parameters were evaluated to optimize the adsorption process, including pH (2-12), concentration (0.1-5 ppm), temperature (25-50 °C), and contact time (5-480

min). Kinetic, isothermal, and thermodynamic analyses were conducted to gain a comprehensive understanding of the adsorption mechanism and equilibrium. Additionally, spectroscopic, DFT calculations and MD simulation were employed to explore the interaction between paracetamol and g-C_3N_4 during adsorption.

2. Experimental Section

2.1. Chemicals: All chemicals employed in this investigation were commercially accessible and exhibited high purity. Melamine (99.8%), sodium hydroxide (99%), hydrochloric acid (37%), methanol (99.5%), isopropanol (99.5%), ethanol (99.5%), and paracetamol (99.9%) were utilized. Deionized water (DIW) was the solvent for preparing the Paracetamol stock solution.

2.2. Synthesis of SNP-g-C_3N_4: Bulk g-C_3N_4 was synthesized by heating 10 grams of melamine in a ceramic crucible at 520°C for 4 hours in a digital furnace, using a heating rate of 5°C per minute. To produce g-C_3N_4 nanosheets, 100 milligrams of bulk g-C_3N_4 were dispersed in 1000 milliliters of a 3:1 isopropanol-to-water mixture. The suspension was then sonicated for 24 hours at room temperature. After centrifugation and washing with deionized water (3 times) and ethanol (1 time), the nanosheets were dried in an oven at 100°C for 6 hours.

2.3. Preparations of paracetamol solutions: 0.2 grams of paracetamol were precisely weighed and dissolved in 200 milliliters of DDW. The solution was then sonicated for 30 minutes to ensure complete dissolution and homogeneity. This stock solution was subsequently used to prepare solutions of varying concentrations (0.1, 0.3, 0.5, 1, 1.5, 3, and 5 ppm) in 100-milliliter volumetric flasks using DIW. A UV-visible spectrophotometer was employed to determine the concentration profile of paracetamol at its maximum absorbance wavelength (λmax) of 249 nanometers.

2.4. Adsorption Optimization and Analysis: To determine optimal adsorption conditions, a series of experiments were conducted using a one-factor-at-a-time approach. Variables explored included pH (2-12), g-C_3N_4 dose (10 mg /10 mL), contact time (5-180 minutes), and temperature (25-50 °C). Drug solutions were prepared in separate glass flasks and incubated with the desired adsorbent dose. After reaching equilibrium, the solutions were centrifuged and filtered before analysis. The adsorption capacity (q_e), and adsorption efficiency (%R_e) were calculated using **Equations** (**1**, and **2**). To identify the rate-limiting step, kinetic studies were conducted. The adsorption rate of paracetamol was determined by quantifying the adsorbed amount at varying time intervals (q_t). **Equation** (**3**) was used for this calculation.

$$q_e = \frac{(C_0 - C_e)}{C_0} \times \frac{V}{W} \quad (1)$$

$$\%R_e = \frac{(C_0 - C_e)}{C_0} \times 100 \quad (2)$$

$$q_t = \frac{(C_0 - C_t)}{C_0} \times \frac{V}{W} \quad (3)$$

Where C_o is the Initial drug concentration (mg/L), C_e is the Equilibrium drug concentration (mg/L), V is Solution volume (L), q_t is the adsorbed amount (mg/g), C_t is the concentration at time t (mg/L), and W is Adsorbent weight (g).

2.5. Instrumentation: To elucidate the structural and morphological properties of the synthesized g-C_3N_4 nanosheets, a suite of characterization techniques was employed. Crystal Structure: XRD using a Shimadzu XRD-LabX-600 diffractometer with Cu Kα radiation (λ = 1.54056 Å) was utilized to assess the crystalline structure. The operating conditions were set at 40 mA/30 kV, with a scanning range of 2θ = 5-80° and a scan speed of 2° per minute. Morphology: TEM using a JEOL JEM-2100F HRTEM operated at 120 kV provided further insights into the nanosheets' morphology. A 1 µL aliquot of the suspension in methanol was placed on a Cu grid and dried under vacuum at 80°C overnight before TEM analysis. Functional Groups: FTIR using a Shimadzu Prestige 21 instrument was employed to identify and characterize functional groups present on the nanoparticles in the range of 450-4000 cm^{-1}. Optical Properties: UV-Vis absorbance spectra were recorded using an Agilent HP-8453 optics system equipped with a Hydrogen-Deuterium lamp for ultraviolet light and a Tungsten lamp for visible light.

2.6. Computational Study: DFT calculations, performed using the DMol3 module of the Materials Studio software (V2022) with the generalized gradient approximation (GGA) function at Perdew–Burke–Ernzerh (PBE) level for optimization, and MD simulation (Adsorption locator) module was employed to investigate the adsorption of drugs onto graphitic carbon nitride (g-C_3N_4).[15, 16] This research aimed to understand the underlying interaction mechanisms and optimize g-C_3N_4 for environmental applications.

3. Results and Discussions

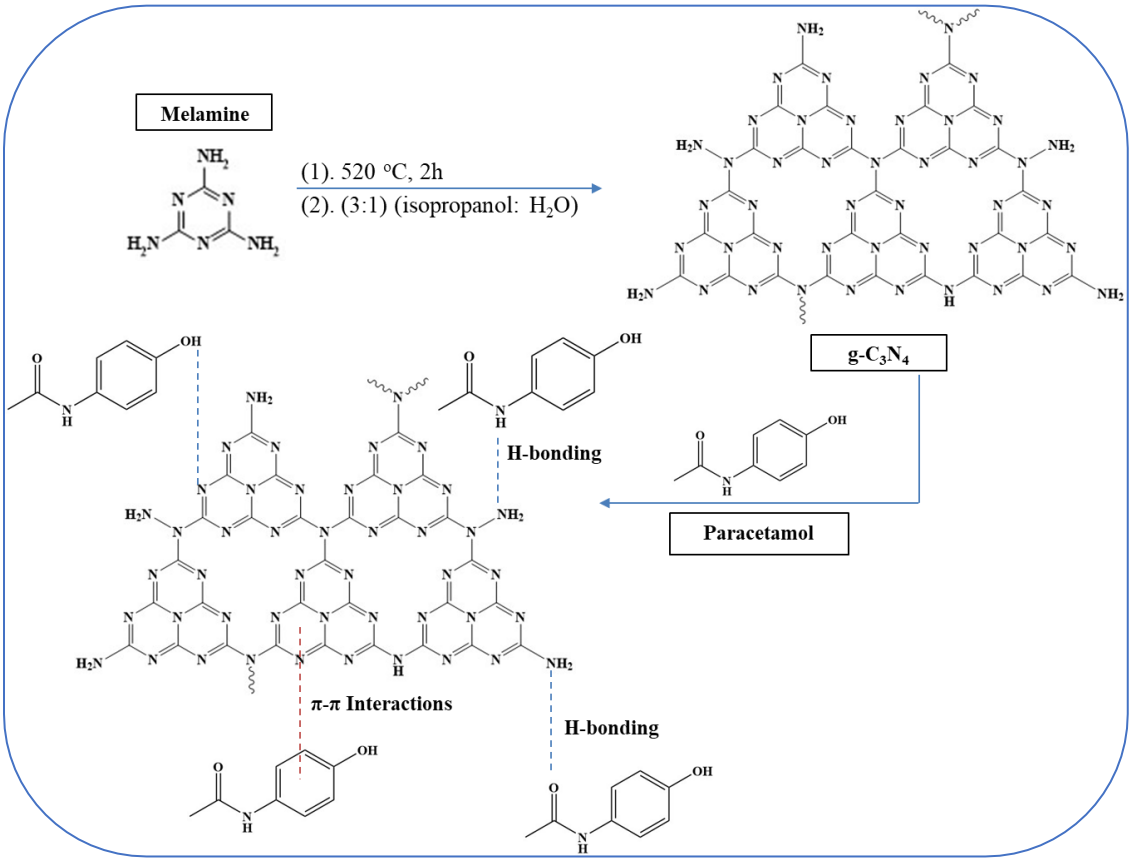

Scheme 1. Procedure to prepare g-C_3N_4 from melamine by thermal decomposition at 520 °C and the possible pathways for paracetamol adsorption.

3.1. Material Design and Characterizations: g-C_3N_4 can be synthesized from melamine through a thermal decomposition process at 520°C as summarized in **Scheme 1**. This reaction involves the condensation and polymerization of melamine molecules, forming a highly conjugated polymer structure. The resulting g-C_3N_4 material exhibits a layered structure similar to graphite, with its unique electronic properties and large surface area making it an excellent candidate for various applications, including adsorption.[12, 17] The ability of g-C_3N_4 to absorb paracetamol is due to its polar surface and the presence of nitrogen-containing functional groups, which can interact with the polar functional groups of paracetamol. This interaction, mainly through hydrogen bonding and dipole-dipole forces, enables the effective adsorption of acetaminophen molecules onto the surface of g-C_3N_4. In addition, π-π interactions between the electron-rich π systems of aromatic rings can contribute to the adsorption process. These interactions can occur in either a parallel or perpendicular arrangement. Hydrogen bonding is a strong dipole-dipole interaction between a hydrogen atom bonded to a highly electronegative atom (e.g., oxygen, nitrogen) and another electronegative atom.[8, 18]

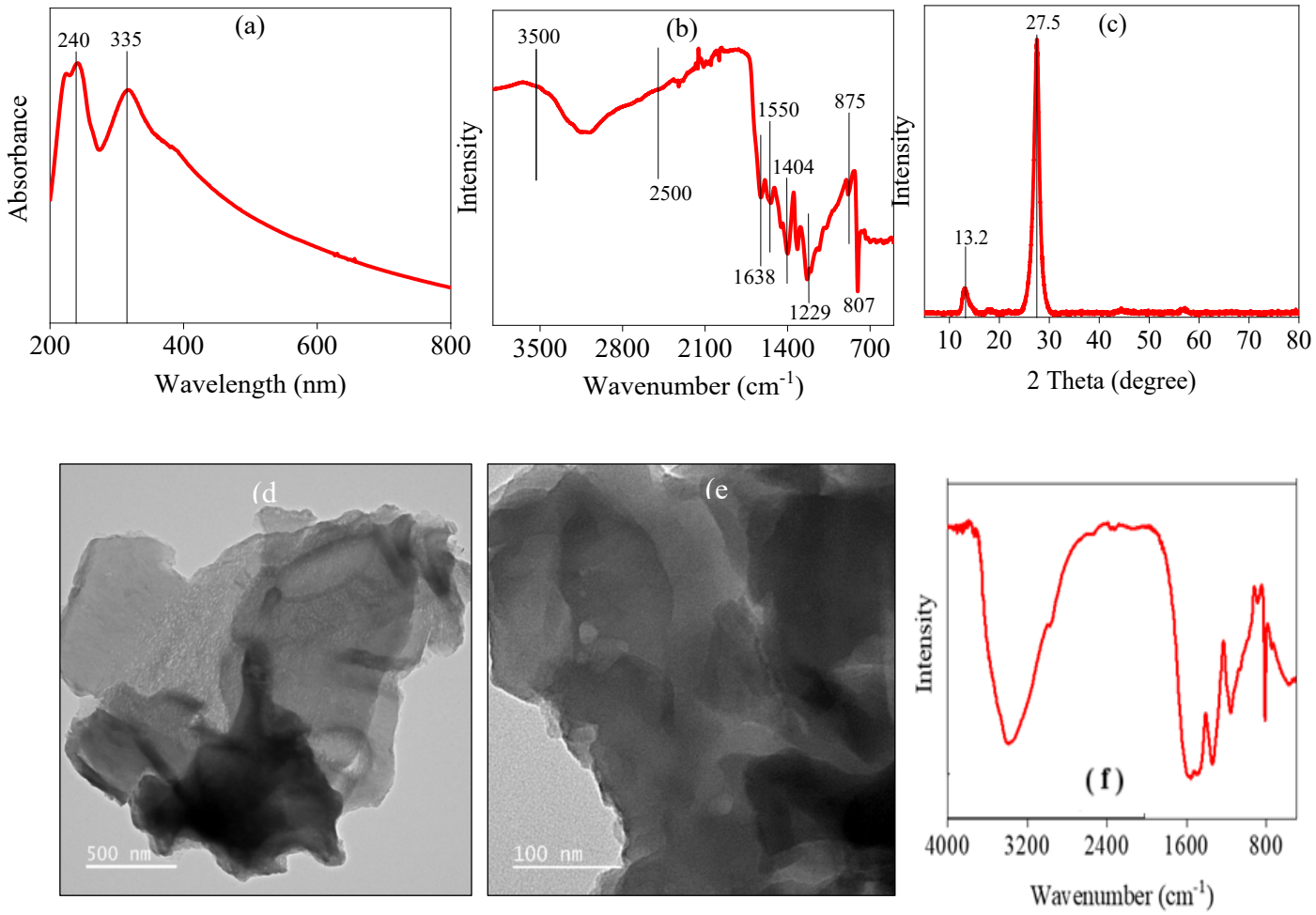

Figure 1. Characterization of g-C_3N_4: (**a**) UV-Vis spectrum, (**b**) FTIR spectrum of g-C_3N_4, (**c**) XRD patterns, (**d, e**) TEM images and (**f**) FTIR spectrum of g-C_3N_4 after adsorption of paracetamol.

3.2. Adsorbent Characterization: The synthesized g-C_3N_4 was characterized using various analytical techniques, including UV-VIS, FTIR, XRD, and TEM. UV-Vis spectroscopy was employed to determine its electronic properties. As shown in **Figure 1a**, the UV-Vis spectrum of g-C_3N_4 exhibits absorption peaks characteristic of a semiconductor, with wavelengths ranging from 200 to 450 nm. These peaks are attributed to the transfer of electrons from the nitrogen 2p orbitals in the valence band to the carbon 2p orbitals in the conduction band. Additionally, a sharp peak at 240 nm is associated with (n to π^*) transitions, while another peak at 335 nm is due to (n to π^*) transitions arising from electron transfer from nitrogen nonbonding orbitals to aromatic anti-bonding orbitals.[13, 19] FTIR spectroscopy was used to characterize the surface functional groups of g-C_3N_4. As depicted in **Figure 1b**, the FTIR spectrum of g-C_3N_4 showed two prominent peaks at 813 and 886 cm^{-1} indicative of triazine ring vibrations. C-N stretching vibrations were confirmed by peaks around 1630-1640 cm^{-1} and 1500-1550 cm^{-1}. C-H stretching vibrations, if present, may be observed around 3200-3400 cm^{-1}. Similarly, N-H stretching vibrations can be detected around 3300-3500 cm^{-1} if amino or imino groups are present. XRD analysis

was conducted to investigate the crystallinity of g-C_3N_4.[20, 21] As shown in **Figure 1c**, the XRD pattern revealed sharp peaks, indicating a crystalline structure. A prominent peak at $2\theta = 28.0°$ corresponds to the stacking of (022) planes, while a weaker peak at $2\theta = 13.3°$ is attributed to the (100) planes of heptazine repeating units in g-C_3N_4. The morphology of g-C_3N_4 was examined using TEM. As depicted in **Figures 1d** and **1e**, the TEM images revealed a sheet-like structure for the g-C_3N_4 nanosheets. These thin, flat sheets often stack on top of each other, forming a layered structure reminiscent of graphite.[12, 18]. After paracetamol adsorption (**Figure 1f**), the FTIR spectrum reveals notable changes, confirming interactions between paracetamol and g-C_3N_4. A new band near 1660 cm^{-1} appears, corresponding to the C=O stretch of the amide group in paracetamol. The broad band between 3000–3500 cm^{-1}, associated with O–H and N–H stretching, shows increased intensity and a slight shift, suggesting hydrogen bonding between paracetamol's phenolic group and nitrogen sites on g-C_3N_4. Additional bands emerge at 1590 cm^{-1} and 1500 cm^{-1}, likely due to aromatic ring vibrations from paracetamol, while the band at 1230 cm^{-1} may arise from C–O stretching in the phenolic group. These modifications—new peaks, shifted intensities, and altered band positions—collectively demonstrate successful paracetamol adsorption. The interactions likely involve hydrogen bonding (e.g., O–H···N or N–H–N) and π–π stacking between paracetamol's aromatic ring and g-C_3N_4's conjugated structure.

3.3. Adsorption Results

3.3.1. The Effect of Initial pH: The point of zero charge (PZC) of g-C_3N_4 at 4.3 (**Figure 2a**) indicates that its surface is positively charged at pH values below 4.3 and negatively charged above it. Paracetamol, being a weak acid with a pK_a around 9.5, primarily exists in its neutral form at pH values below its pK_a. As the pH increases towards the PZC, the positive surface charge of g-C_3N_4 decreases, reducing electrostatic repulsion and promoting adsorption. This is evident in **Figure 2b**, where the adsorption efficiency (R_e) increases significantly as the pH approaches the PZC. However, at pH values significantly above the PZC, the negatively charged g-C_3N_4 surface may repel the anionic form of paracetamol, which starts to form as the pH approaches the pK_a of paracetamol. This leads to a decrease in adsorption efficiency, as observed in **Figure 2b** at higher pH values. Therefore, the optimal pH for paracetamol adsorption onto g-C_3N_4 lies around the PZC, where the balance between electrostatic interactions and other adsorption mechanisms is favorable. This optimal pH range is approximately 4-6, as indicated by the peak in the adsorption efficiency curve in **Figure 2b**.[22, 23]

3.3.2. The Effect of Concentration and Adsorption Isotherms: To investigate the adsorption capacity of g-C_3N_4 for paracetamol, experiments were carried out at varying initial concentrations. As depicted in **Figure 2c**, the amount of paracetamol adsorbed increased with increasing initial concentration, reaching a maximum of 1.11 mg/g. This trend can be explained by the Langmuir adsorption isotherm, which is expressed by **Equation 4**.[24]

$$\frac{1}{q_e} = \frac{1}{bq_m} + \frac{1}{q_m}C_e \tag{4}$$

$$R_L = \frac{1}{1 + bC_0} \tag{5}$$

Where: C_e is the equilibrium concentration of the solute (mg/L), q_e is the amount of solute adsorbed per unit mass of adsorbent (mg/g), b is Langmuir constant related to the affinity between the adsorbent and adsorbate (L/mg), q_m is the maximum adsorption capacity (mg/g). The dimensionless equilibrium parameter (R_L) is a crucial characteristic of the Langmuir isotherm, given by **Equation 5**.[25]

Table 1. Parameters of the Langmuir-isotherms model for the Adsorption of paracetamol on g-C_3N_4.

R^2	b (L/mg)	$q_{max, fitted}$	q_{exp}	R_L
0.9998	76.69	1.10	1.11	0.012

The experimental data exhibited excellent agreement with the Langmuir model, as shown in **Figure 2d** and **Table 1**. The high correlation coefficient ($R^2 = 0.9998$) and favorable R_L values ($0 < RL < 0.1$) further support the Langmuir model's applicability. The calculated maximum adsorption capacity (q_{max}) from the Langmuir model (1.10 mg/g) is in close agreement with the experimental data (1.1 mg/g), reinforcing the monolayer adsorption mechanism. The exceptional adsorption performance of g-C_3N_4 for paracetamol can be attributed to its high surface area and the presence of nitrogen-containing functional groups, such as amino groups. These functional groups facilitate strong hydrogen bonding and electrostatic interactions with paracetamol, leading to efficient adsorption.

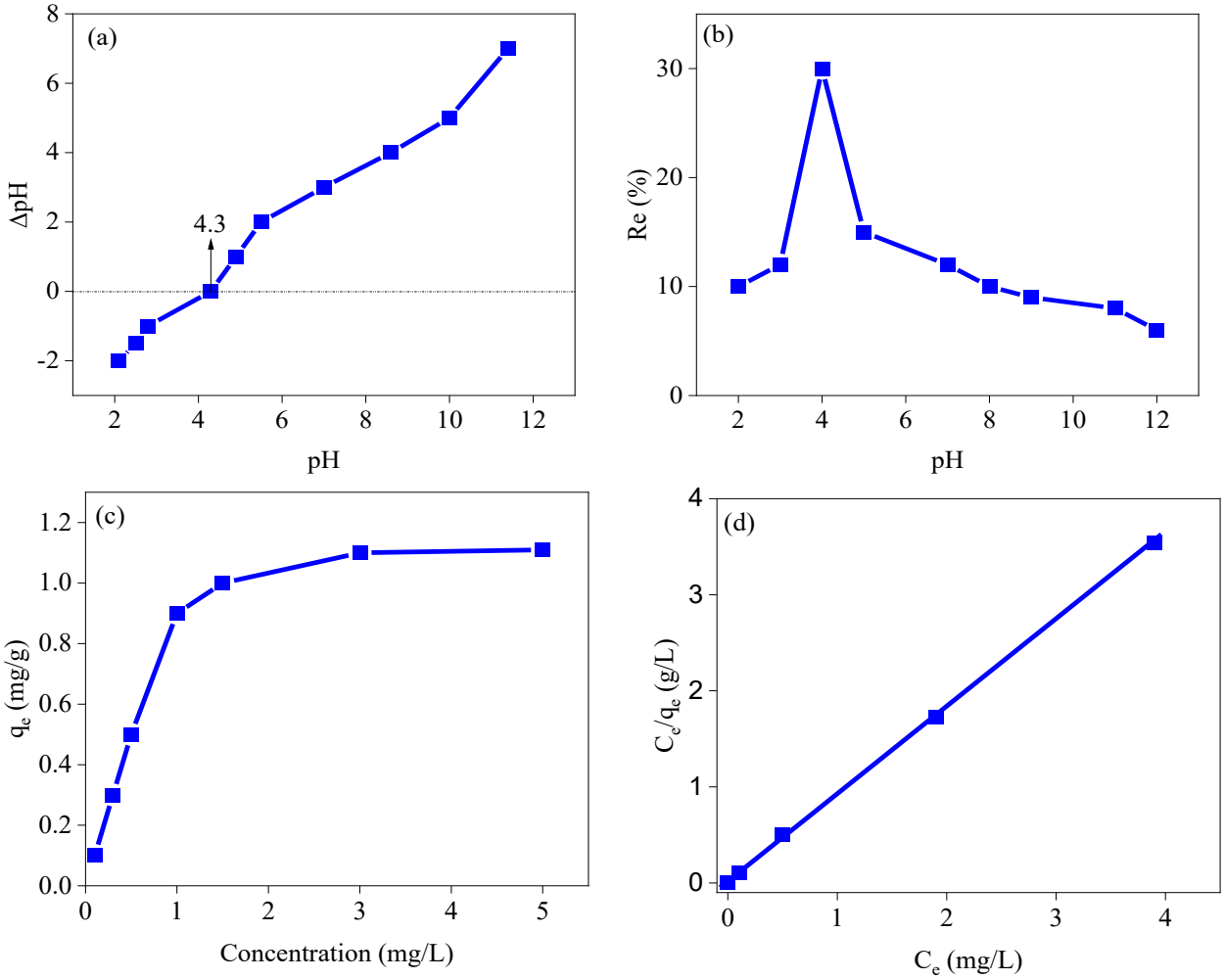

Figure 2. The effect of pH on the adsorption of paracetamol onto g-C_3N_4. (**a**) shows the point of zero charge (PZC) of g-C_3N_4, which is 4.3. (**b**) shows the adsorption efficiency of paracetamol onto g-C_3N_4 as a function of pH. (**c**) the effect of concentration on the adsorption of paracetamol onto g-C_3N_4 [Conditions: C_0 = 0.1, 0.3, 0.5, 1, 1.5, 3, 5 ppm, pH = 4, T = 298 K, t = 420 min, adsorbent dose = 0.01 g/10 mL]. (d) Langmuir isotherm model for the adsorption.

3.3.3. The Effect of Contact Time and Adsorption Kinetics: Adsorption is a time-dependent process, and the impact of contact time can significantly influence the overall efficiency. This study investigated the effect of contact time within 30 to 180 minutes. As illustrated in **Figure 3a**, the adsorption rate was initially slow, but accelerated notably after 15 minutes, reaching equilibrium at approximately 60 minutes. Beyond this point, no further adsorption was observed, and even desorption might have occurred. This behavior can be attributed to the gradual saturation of active sites on the adsorbent surface. As the surface becomes increasingly occupied, the availability of free sites decreases, leading to a decline in the adsorption rate.[9, 26] Kinetic modeling was employed to gain insights into the underlying mechanisms of the adsorption process. The pseudo-second-order kinetic model was used as in **Equation 6**. Where: k_2

($g.mole^{-1}.min^{-1}$) is the second-order rate constant of adsorption, qe and q_t are the adsorbed amount (mg/g) at equilibrium and at time t (min), respectively.[24]

$$\frac{t}{q_t} = \frac{1}{k_2 q_e^2} + \frac{t}{q_e} \quad (6)$$

The results in **Figure 3b** and **Table 2** best fit the experimental data, as evidenced by the high correlation coefficient ($R^2 = 0.9866$) and the close agreement between the calculated and experimental equilibrium adsorption capacities ($q_{e,\,fitted,}$ and $q_{e,\,exp}$). This suggests that the rate-limiting step in the adsorption process involves the interaction between the adsorbate molecules and the active sites on the adsorbent surface.

Table 2. Kinetic Parameters for Adsorption of Paracetamol on g-C_3N_4.

R^2	$q_{max,\,fitted}$	q_{exp}	k_2
0.9866	0.568	0.500	0.10173

3.3.4. The Effect of Temperature and Adsorption Thermodynamics: The impact of temperature on the adsorption capacity of paracetamol onto g-C_3N_4 was investigated. Experiments were conducted at pH 4, with a contact time of 420 minutes, a g-C_3N_4 dosage of 10 mg/L, and paracetamol concentrations ranging from 0.1 to 5 mg/L. Three temperatures were tested: 25, 35, and 50 °C. As the temperature increased, the maximum adsorption capacity rose from 1.1 to 3.2 mg/g as **Figure 3c** shows, likely due to increased molecular mobility and kinetic energy at higher temperatures.[26] Thermodynamic parameters (ΔH, ΔS, and ΔG) were determined using **Equations 7 and 8**. Where ΔG° represents the change in free energy, ΔH° represents the change in enthalpy, ΔS° represents the change in entropy, R is the gas constant, T is the temperature, and K_c is the equilibrium constant.[27, 28]

$$\Delta G^{\circ} = -RT \ln K_c \quad (7)$$

$$\ln K_c = \left(\frac{\Delta S^{\circ}}{R}\right) - \left(\frac{\Delta H^{\circ}}{R}\right)\frac{1}{T} \quad (8)$$

The data and the calculated thermodynamic parameters are presented in **Figure 3d** and **Table 3**, respectively. The negative ΔG values indicate that the adsorption process is spontaneous and favorable at all temperatures, with the process becoming more favorable at higher temperatures. This suggests a potential expansion of adsorbent pores at higher temperatures, facilitating increased diffusion of paracetamol molecules. The positive ΔH value confirms the endothermic nature of the process, consistent with the increased adsorption capacity at higher temperatures. Additionally, the positive ΔS value suggests an increase in disorder at the solid-solution interface during adsorption.[23, 26] These findings indicate a strong affinity between paracetamol and the g-C_3N_4 adsorbent, with the adsorption mechanism primarily physical in nature.

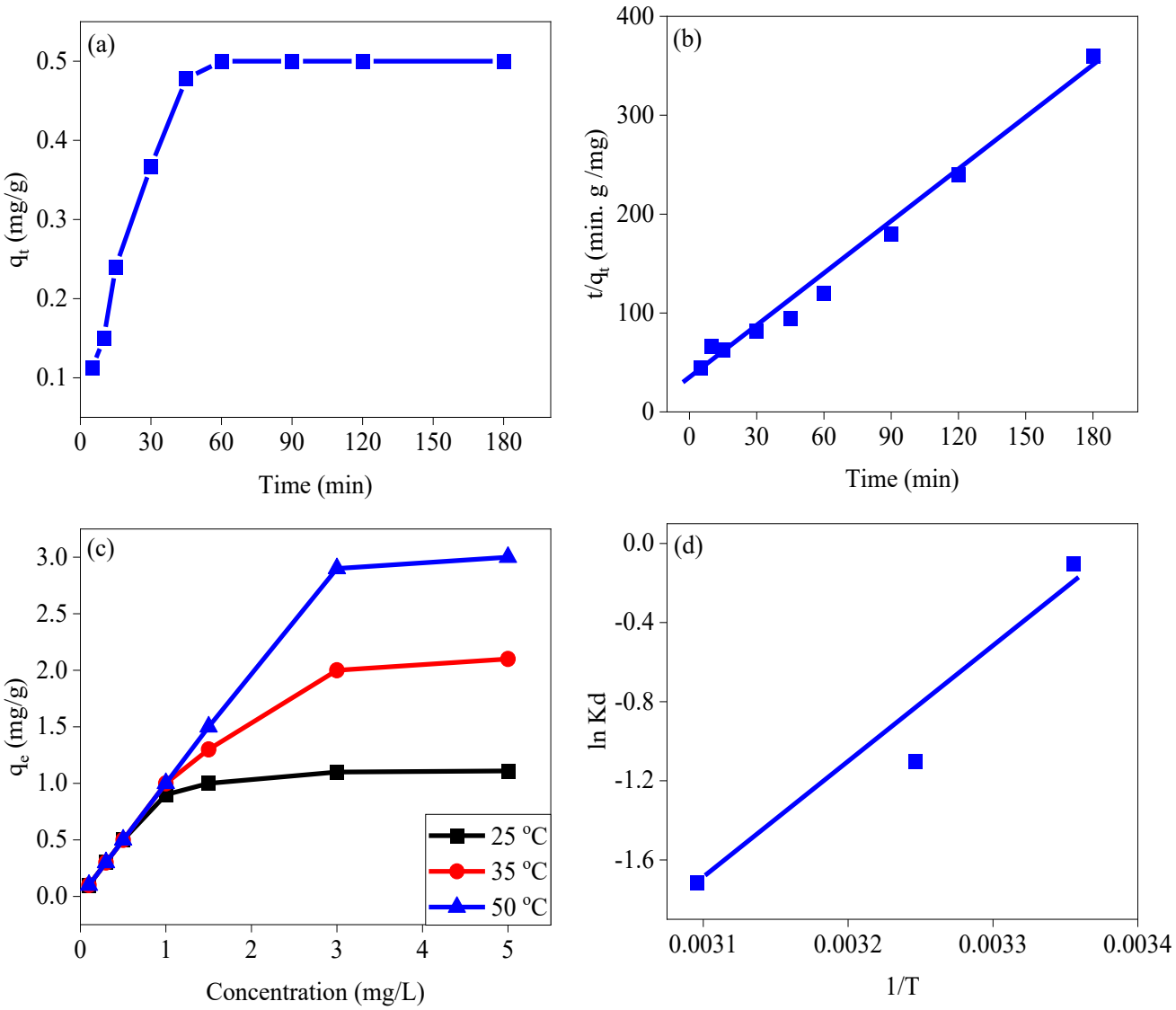

Figure 3: (**a**) Impact of contact time on paracetamol removal by g-C_3N_4 (pH 4, adsorbent dose = 0.001 g/10 mL, T = 298 K). (**b**) Pseudo-second-order kinetic model for paracetamol adsorption onto g-C_3N_4. (**c**) Influence of temperature on paracetamol removal by g-C_3N_4 (pH 4, adsorbent dose = 0.001 g/10 mL, T = 298, 308, 323 K, t = 420 min). (**d**) Thermodynamic assessment via Van't Hoff plot reveals the endothermic nature of paracetamol adsorption on g-C_3N_4 ($\Delta H° > 0$).

Table 3: Thermodynamic parameters for the adsorption of paracetamol on g-C_3N_4.

ΔG (kJ mol^{-1})			**ΔH (kJ mol^{-1})**	**ΔS (kJ mol^{-1} T^{-1})**	**R^2**
298 K	308 K	323 K	48.356	0.1509	0.9987
-21.059	-23.456	-27.525			

3.5. Theoretical calculation Results: DFT was employed to investigate the adsorption of drugs onto g-C_3N_4,[29-32] aiming to elucidate the underlying interaction mechanisms and optimize this material for environmental remediation applications. The favorable interaction between g-C_3N_4 and paracetamol is likely attributed to the unique surface chemistry and structural features of g-C_3N_4, which enhance its affinity for organic molecules.[33] Structural interactions between paracetamol and g-C_3N_4 are likely mediated through π-π stacking and hydrogen bonding, with the triazine groups of g-C_3N_4 playing a crucial role in governing the adsorption efficiency. DFT provides valuable insights into the stability and electronic properties of the g-C_3N_4-drug complex. The calculations reveal that adsorption induces alterations in electron density and facilitates charge transfer, which is critical for understanding the adsorption process and optimizing g-C_3N_4 for efficient drug removal from water.[32, 34].

Table 4: DFT calculated parameters from Optimization processes for Paracetamol, g-C_3N_4, and Paracetamol-g-C_3N_4 complex.

Parameter		**g-C_3N_4**	**Paracetamol**	**g-C_3N_4-Paracitamol complex**
(E_{LUMO})	E_{HOMO}	-5.706	-4.921	-5.031
(E_{HOMO})	E_{LUMO}	-3.436	-1.12	-3.481
(ΔEg)	$\Delta E_{(HOMO-LUMO)}$	-2.27	-3.801	-1.55
(I)	Ionization energy (I)	5.706	4.921	5.031
(A)	Electron affinity (A)	3.436	1.12	3.481
(η)	Electronegativity (X)	4.571	3.021	4.256
(χ)	Global hardness (η)	1.135	1.901	0.775
(μ)	Chemical potential (μ)	-4.571	-3.021	-4.256
(σ)	Global softness (σ)	0.881	0.526	1.290
(ω)	Global electrophilicity (ω)	9.204	2.400	11.686
(ω +)	Electroaccepting (ω+) power	7.061	1.128	9.655
(ω -)	Electrodonating (ω-) power	11.632	4.148	13.911
(ω ±)	Net electrophilicity (Δω+-)	18.692	5.276	23.566
(ε)	Nucleophilicity (ε)	0.109	0.417	0.086
(Q_{max})	Fraction of transferred electrons (ΔN)	-2.014	-0.795	-2.746
(ΔN)	Electronic charge accepting capability Qmax	4.027	1.589	5.492
E_f	Formation energy (eV)	-490.217	-101.818	-591.031

Table 4 summarizes the electronic parameters derived from the optimization of paracetamol, g-C_3N_4, and their complex. The data reveals that the interaction between g-C_3N_4 and paracetamol results in shifts in both the highest occupied molecular orbital (HOMO) and lowest unoccupied molecular orbital (LUMO) energies, signifying a modification of the electronic structure upon complexation. The observed decrease in the energy gap (ΔE_g) between HOMO and LUMO for the complex suggests the formation of a more stable compound with lower energy. The ionization energy of the complex lies between those of paracetamol and g-C_3N_4, indicating a balanced electronic interaction. Conversely, the electron affinity of the complex is closer to that of g-C_3N_4, suggesting that g-C_3N_4 primarily governs the electron-accepting behavior of the complex. The reduced global hardness of the complex implies increased reactivity and a higher likelihood of interaction. Its electronegativity falls within an intermediate range, signifying a balanced distribution of electron density. The complex's chemical potential aligns more closely with that of g-C_3N_4, indicating that g-C_3N_4 exerts a significant influence on the overall chemical behavior of the complex. Furthermore, the increased global softness of the complex suggests enhanced reactivity and flexibility. The elevated net electrophilicity of the complex points towards a higher overall reactivity. Conversely, the observed decrease in nucleophilicity implies a reduced tendency to donate electrons in the complex.

Table 5 . Lower adsorption configuration output results from the Adsorption Locator model**.**

Structures	**Total energy** $\boldsymbol{kcal\ mol^{-1}}$	$\boldsymbol{Adsorption\ energy}$ $\boldsymbol{kcal\ mol^{-1}}$	**Rigid adsorption energy** $\boldsymbol{kcal\ mol^{-1}}$	**Deformation energy** $\boldsymbol{kcal\ mol^{-1}}$	$\boldsymbol{dE_{ad}/dN_i}$ $\boldsymbol{kcal\ mol^{-1}}$
Paracetamol + g-C_3N_4	-85.696×10^3	-38.640×10^3	-36.000×10^3	-2.643	-38.640

The adsorption study reveals an electrostatic attraction between paracetamol and the g-C_3N_4 surface, evidenced by an increase in the bond lengths of NH and CN groups within g-C_3N_4 due to the interaction with paracetamol. The formation of hydrogen bonds (Paracetamol) N-H...N-H (g-C_3N_4) is likely, supported by the short distances observed between the nearest H and N atoms (1.678, 3.079, and 2.786 Å) after adsorption, as depicted in **Figure 4,** which confirms the FTIR results shown in **Figure 1f**. MD simulations indicate a strong interaction between paracetamol and g-C_3N_4, corroborated by the parameter analysis. The negative values for total energy, adsorption energy, and rigid adsorption energy in **Table 5** suggest a stable complex with strong intermolecular interactions. Furthermore, the low deformation energy confirms the stability of the complex by indicating minimal structural changes in the molecules during adsorption. These computational results are consistent with the experimental findings.

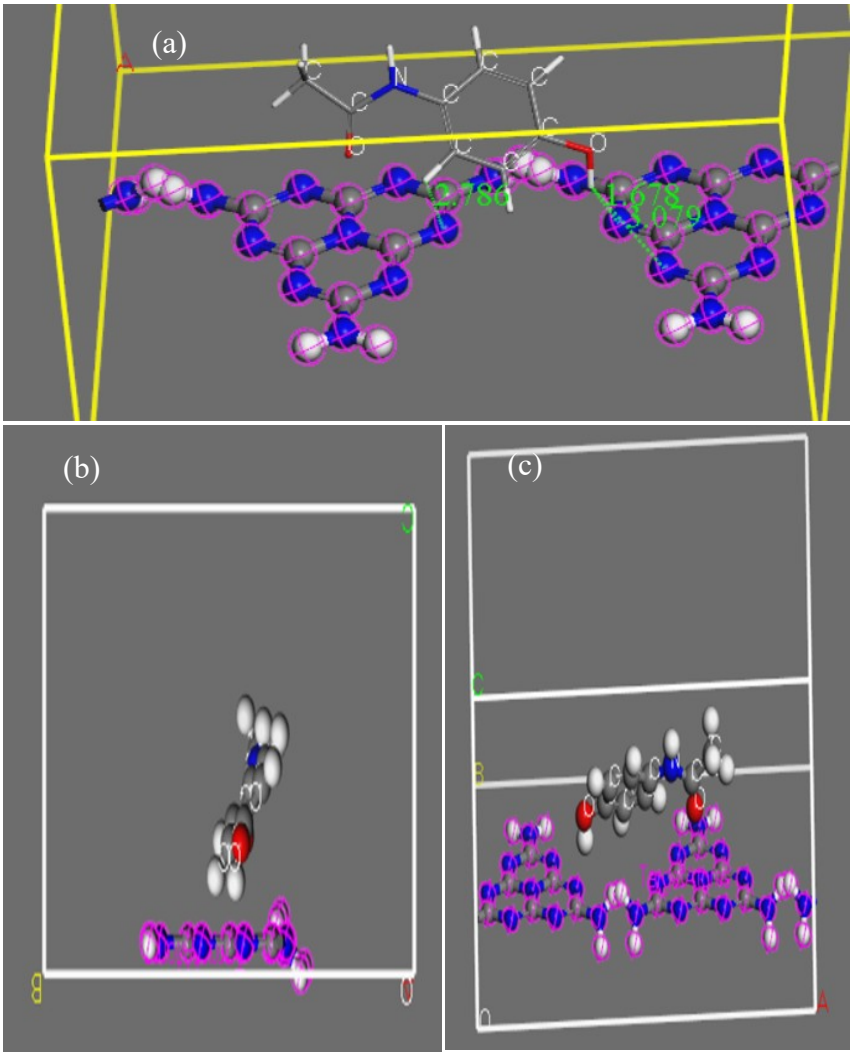

Figure 4. (**a**) The obtained energies for the most stable complex, (**a**) top view and (**b**) side view of the adsorption adsorbed paracetamol-g-C_3N_4 complex.

4. Conclusions and Outlooks

This study successfully demonstrated the feasibility of employing cost-effective raw graphitic carbon nitride for paracetamol removal from water. Comprehensive material characterization via XRD, XRF, FT-IR, and TEM elucidated the adsorbent's properties. Systematic investigation of key operational parameters, including pH, contact time, adsorbent dosage, and initial paracetamol concentration, revealed a maximum adsorption capacity of 1.1 mg/g achieved at 25°C within 60 minutes. The adsorption process was well-described by both Langmuir and pseudo-second-order kinetic models. Complementary DFT

calculations confirmed the stability of the paracetamol-g-C_3N_4 complex, while MD simulations indicated a high propensity for hydrogen bond formation, yielding a calculated adsorption energy of –38.640 x 10^{-3} kcal/mol. The strong synergy between these experimental and computational findings highlights the significant potential of raw graphitic carbon nitride as an environmentally benign and economical adsorbent for pharmaceutical contaminant removal from aqueous solutions. Future research should explore its efficacy in treating real wastewater samples and investigate the regeneration capabilities of the spent adsorbent to further establish its practical applicability.

References

[1] Hejna, M., D. Kapuścińska, and A. Aksmann, *Pharmaceuticals in the Aquatic Environment: A Review on Eco-Toxicology and the Remediation Potential of Algae.* Int J Environ Res Public Health, 2022. **19**(13).

[2] Eapen, J.V., et al., *A review of the effects of pharmaceutical pollutants on humans and aquatic ecosystem.* Exploration of Drug Science, 2024. **2**(5): p. 484-507.

[3] Quesada, H.B., et al., *Surface water pollution by pharmaceuticals and an alternative of removal by low-cost adsorbents: A review.* Chemosphere, 2019. **222**: p. 766-780.

[4] Pacheco-Álvarez, M., et al., *A critical review on paracetamol removal from different aqueous matrices by Fenton and Fenton-based processes, and their combined methods.* Chemosphere, 2022. **303**: p. 134883.

[5] Al-howri, B.M., et al., *Paracetamol in diverse water sources: health hazards and treatment efficacy emphasizing adsorption techniques—a review.* International Journal of Environmental Science and Technology, 2024. **21**(15): p. 9743-9762.

[6] Ivanova, D., G. Tzvetkov, and N. Kaneva *Degradation of Paracetamol in Distilled and Drinking Water via Ag/ZnO Photocatalysis under UV and Natural Sunlight*. Water, 2023. **15**, DOI: 10.3390/w15203549.

[7] Islam, M., et al., *Adsorptive removal of paracetamol from aqueous media: A comprehensive review of adsorbent materials, adsorption mechanisms, recent advancements, and future perspectives.* Journal of Molecular Liquids, 2024.

[8] Aminul Islam, M., et al., *Adsorptive removal of paracetamol from aqueous media: A review of adsorbent materials, adsorption mechanisms, advancements, and future perspectives.* Journal of Molecular Liquids, 2024. **396**: p. 123976.

[9] Spaltro, A., et al., *Removal of paracetamol from aqueous solution by activated carbon and silica. Experimental and computational study.* Journal of Contaminant Hydrology, 2021. **236**: p. 103739.

[10] Maneewong, Y., et al., *Paracetamol removal from water using N-doped activated carbon derived from coconut shell: Kinetics, equilibrium, cost analysis, heat contributions, and molecular-level insight.* Chemical Engineering Research and Design, 2022. **185**: p. 163-175.

[11] Yılmaz, Ş., A. Zengin, and T. Şahan, *Effective utilization of Fe(III)-based metal organic framework-coated cellulose paper for highly efficient elimination from the liquid phase of paracetamol as a pharmaceutical pollutant.* Environmental Technology & Innovation, 2021. **24**: p. 101799.

[12] Zhao, Z., Y. Sun, and F. Dong, *Graphitic carbon nitride based nanocomposites: a review.* Nanoscale, 2015. **7**(1): p. 15-37.

[13] Zhao, G.-Q., et al., *A critical review on graphitic carbon nitride (g-C3N4)-based composites for environmental remediation.* Separation and Purification Technology, 2021. **279**: p. 119769.

[14] Alaghmandfard, A. and K. Ghandi, *A Comprehensive Review of Graphitic Carbon Nitride (g-C3N4)–Metal Oxide-Based Nanocomposites: Potential for Photocatalysis and Sensing.* Nanomaterials, 2022. **12**(2): p. 294.

[15] Bicheng, Z., et al., *Adsorption investigation of CO 2 on g-C 3 N 4 surface by DFT calculation.* Journal of CO2 Utilization, 2017. **21**: p. 327-335.

[16]Iqbal, J., et al., *DFT study of therapeutic potential of graphitic carbon nitride (g-C3N4) as a new drug delivery system for carboplatin to treat cancer.* Journal of Molecular Liquids, 2021. **331**: p. 115607.
[17]Zhu, J., et al., *Graphitic Carbon Nitride: Synthesis, Properties, and Applications in Catalysis.* ACS Applied Materials & Interfaces, 2014. **6**(19): p. 16449-16465.
[18]Fronczak, M., *Adsorption performance of graphitic carbon nitride-based materials: Current state of the art.* Journal of Environmental Chemical Engineering, 2020. **8**(5): p. 104411.
[19]Ghalkhani, M., M.H. Khaneghah, and E. Sohouli, *Chapter 13 - Graphitic carbon nitride: Synthesis and characterization*, in *Handbook of Carbon-Based Nanomaterials*, S. Thomas, et al., Editors. 2021, Elsevier. p. 573-590.
[20]Sunasee, S., et al., *Sonophotocatalytic degradation of bisphenol A and its intermediates with graphitic carbon nitride.* Environmental Science and Pollution Research, 2019. **26**: p. 1-12.
[21]Ahmaruzzaman, M. and S.R. Mishra, *Photocatalytic performance of g-C3N4 based nanocomposites for effective degradation/removal of dyes from water and wastewater.* Materials Research Bulletin, 2021. **143**: p. 111417.
[22]Bernal, V., et al., *Effect of Solution pH on the Adsorption of Paracetamol on Chemically Modified Activated Carbons.* Molecules, 2017. **22**: p. 1032.
[23]Terzyk, A.P., *The influence of activated carbon surface chemical composition on the adsorption of acetaminophen (paracetamol) in vitro: Part II. TG, FTIR, and XPS analysis of carbons and the temperature dependence of adsorption kinetics at the neutral pH.* Colloids and Surfaces A: Physicochemical and Engineering Aspects, 2001. **177**(1): p. 23-45.
[24]Azizian, S. and S. Eris, *Chapter 6 - Adsorption isotherms and kinetics*, in *Interface Science and Technology*, M. Ghaedi, Editor. 2021, Elsevier. p. 445-509.
[25]Vedenyapina, M., et al., *Adsorption of Heavy Metals on Activated Carbons (A Review).* Solid Fuel Chemistry, 2021. **55**: p. 83-104.
[26]Awad, F.S., et al., *Thiol- and Amine-Incorporated UIO-66-NH2 as an Efficient Adsorbent for the Removal of Mercury(II) and Phosphate Ions from Aqueous Solutions.* Industrial & Engineering Chemistry Research, 2021. **60**(34): p. 12675-12688.
[27]Allaoui, I., et al., *Adsorption equilibrium, kinetic, and thermodynamic studies on the removal of paracetamol from wastewater using natural and HDTMA-modified clay.* Desalination and Water Treatment, 2024. **318**: p. 100345.
[28]Haro, N.K., et al., *Kinetic, equilibrium and thermodynamic studies of the adsorption of paracetamol in activated carbon in batch model and fixed-bed column.* Applied Water Science, 2021. **11**(2): p. 38.
[29]Perveen, M., et al., *Therapeutic potential of graphitic carbon nitride as a drug delivery system for cisplatin (anticancer drug): A DFT approach.* Biophysical Chemistry, 2020. **267**: p. 106461.
[30]Shamim, M., et al., *DFT study of therapeutic potential of graphitic carbon nitride (g-C3N4) as a new drug delivery system for carboplatin to treat cancer.* Journal of Molecular Liquids, 2021. **331**: p. 115607.
[31]Perveen, M., et al., *DFT study of therapeutic potential of graphitic carbon nitride as a carrier for controlled release of melphalan: an anticancer drug.* Journal of Molecular Modeling, 2022. **28**(11): p. 359.
[32]Negro, P., et al., *Combined DFT-D3 computational and experimental studies on g-C3N4: New insight into structure, optical, and vibrational properties.* Materials, 2023. **16**(10): p. 3644.
[33]Jiménez-Salcedo, M., M. Monge, and M.T. Tena, *An organometallic approach for the preparation of Au–TiO2 and Au-g-C3N4 nanohybrids: improving the depletion of paracetamol under visible light.* Photochemical & Photobiological Sciences, 2022. **21**(3): p. 337-347.
[34]Luo, S., et al., *Effect of Pt doping on sensing performance of g-C3N4 for detecting hydrogen gas: a DFT study.* Vacuum, 2022. **200**: p. 111014.